

Modelling take-off moment arms in an ornithocheiraean pterosaur

Benjamin W Griffin $^{Corresp.,\,1}$, Elizabeth Martin-Silverstone 1 , Rodrigo V Pêgas 2 , Erik Anthony Meilak 3 , Fabiana R Costa 2 , Colin Palmer 1 , Emily J Rayfield 1

Corresponding Author: Benjamin W Griffin Email address: ben.griffin@bristol.ac.uk

Take-off is a vital part of powered flight which likely constrains the size of birds, yet extinct pterosaurs are known to have reached far larger sizes. Three different hypothesised take-off motions (bipedal burst launching, bipedal countermotion launching, and quadrupedal launching) have been proposed as explanations for how pterosaurs became airborne and circumvented this proposed morphological limit. We have constructed a computational musculoskeletal model of a 5 m wingspan ornithocheiraean pterosaur, reconstructing thirty-four key muscles to estimate the muscle moment arms throughout the three hypothesised take-off motions. In all our models we found the muscles utilised in the quadrupedal take-off have the largest moment arms throughout the entire take-off sequences and for the take-off pose.

¹ Palaeobiology Group, School of Earth Sciences, University of Bristol, Bristol, United Kingdom

² Laboratório de Paleontologia de Vertebrados e Comportamento Animal, Universidade Federal do ABC, Alameda da Universidade, s/n, Anchieta, 09606-045, São Bernardo do Campo, SP, Brazil

³ University of Keele, Keele, United Kingdom



Modelling take-off moment arms in an

2 ornithocheiraean pterosaur.

- 3 B. W. Griffin¹, E. Martin-Silverstone¹, R. Pêgas², E. A. Meilak³, F. Costa², C. Palmer¹, E. J.
- 4 Rayfield¹
- ¹ Bristol Palaeobiology Group, School of Earth Sciences, University of Bristol, Life Sciences
- 6 Building, Bristol BS8 1TS, UK.
- 7 ² Laboratório de Paleontologia de Vertebrados e Comportamento Animal, Universidade Federal
- 8 do ABC, Alameda da Universidade, s/n, Anchieta, 09606-045, São Bernardo do Campo, SP,
- 9 Brazil.
- 10 ³ University of Keele, Keele, United Kingdom

11

12 Abstract

Take-off is a vital part of powered flight which likely constrains the size of birds, yet 13 14 extinct pterosaurs are known to have reached far larger sizes. Three different hypothesised take-off motions (bipedal burst launching, bipedal countermotion launching, and quadrupedal 15 16 launching) have been proposed as explanations for how pterosaurs became airborne and 17 circumvented this proposed morphological limit. We have constructed a computational 18 musculoskeletal model of a 5 m wingspan ornithocheiraean pterosaur, reconstructing thirty-four key muscles to estimate the muscle moment arms throughout the three hypothesised take-off 19 motions. In all our models we found the muscles utilised in the quadrupedal take-off have the 20 21 largest moment arms throughout the entire take-off sequences and for the take-off pose.

22



24

25

26

27

28

29

30

31

32

33

34

35

36

37

38

39

40

41

42

43

44

45

46

47

Introduction

Powered flight is a method of locomotion that is limited to very few animals as it is energy intensive and requires specific adaptations to achieve launch, thrust, and lift (Rayner, 1989). The most energy intensive part of powered flight is take-off from the ground as this requires the animal to generate enough velocity to overcome drag and for the wings to start to produce lift (Pennycuick, 1968; Rayner, 1988; Alexander, 1998). The take-off also requires the animal to get high enough into the air to start an unobstructed flapping cycle. No modern flying animal exceeds a mass of 25kg with the heaviest volant living animal, Otis tarda (the Great Bustard), recorded as reaching 22kg (Henderson, 2010). This limit has been previously attributed to the differential in scaling between increases in mass and increases in available muscle power which is predicted to increase at approximately mass^{0.75} (Alexander, 1998). Despite this, many extinct animals have reached greater sizes and are still considered capable of flight, including birds such as Argentavis magnificens and Pelagornis sandersi which are predicted to have masses of 70kg and 21.8-40kg respectively (Goto et al., 2022). Pterosaurs vary in size, with medium sized pterosaurs reaching wingspans between 2 and 5m predicted and masses ranging between 2kg to 30kg (Witton, 2008; Martin-Silverstone, 2017; Goto et al., 2022). Pterosaurs have also reached the largest sizes of any animal considered volant with the largest pterosaurs such as Quetzalcoatlus northropi predicted to have reached much greater masses (150kg, or more commonly 250kg (Witton, 2008; Witton & Habib, 2010; Padian et al., 2021)). Flight at such large body masses challenges our understanding of the functional limits of flight making understanding take-off in pterosaurs crucial to establishing the functional limits of flight in organisms. There are two main hypotheses for how pterosaurs launched. The bipedal launch hypothesis is based on modern bird take-offs while the quadrupedal launch hypothesis is

partially inspired by vampire bat take-offs (Habib, 2008). For an unassisted bipedal take-off,



birds broadly fall into two different motions (Earls, 2000). In the first style, hereafter referred to as the bipedal countermotion take-off, the animal starts in a terrestrial locomotory bipedal pose. As the take-off cycle starts, the animal begins a crouching counter movement where it bends its hindlimbs and lowers its centre of mass while beginning to lean forward. The animal then rapidly extends the wings and hind limbs to launch, pushing the animal forward and upward. This take-off style is more favoured by birds that are less specialised for terrestrial locomotion, for example the European starling *Sturnis vulgaris* (Earls, 2000).

The second take-off motion is hereafter referred to as a bipedal burst take-off. This take-off begins already in a deep crouch and then rapidly extends the hind limbs with the body angled to launch nearly vertically while the wings start their initial downstroke. Because of the near vertical launch trajectory this take-off style results in limited forward motion but reaches greater heights. This style of take-off is favoured by birds that are specialised for living primarily terrestrially and fly rarely such as the European migratory quail *Coturnix coturnix* (Earls, 2000). A proposed mode of take-off was recently proposed for the largest pterosaurs (Padian et al., 2021) which is nearly identical to the bipedal burst take-off. The only substantial difference between the bipedal burst take-off of birds and proposed pterosaur take-off is that pterosaurs could not start to utilise the wings to assist with the take-off until a sufficient height is reached for the wings to clear the ground. The distal wings of pterosaurs were unable to deform in the same manner as the feathers of a bird due to the bony spar that supports the pterosaur wing membrane so any contact with the ground during flapping would have likely damaged the wing (Hone, Van Rooijen & Habib, 2015). As this is the only distinction, we consider this model of pterosaur take-off as a bipedal burst take-off in our analysis.

The quadrupedal launch hypothesis described for pterosaurs is split into three main steps starting from a quadrupedal stance (Habib, 2008; Molnar, 2009; Griffin et al., 2022). The first is a crouching counter movement much like the bipedal take-off. When the deepest part of



the crouch was reached the pterosaur began extending its hindlimbs providing an initial forward impulse and pushing the pterosaur onto its forelimbs. When the hindlimbs leave the ground the vault phase began. During this phase, the hindlimbs assumed the pose utilised in flight and the weight of the animal shifted to be entirely supported by the forelimbs. The launch phase then started as the forelimbs began to extend, pushing the pterosaur upwards and forwards until the forelimbs lost contact with the ground. This differs from a standard vampire bat take-off where the take-off is almost vertical; in vampire bats the launch impulse is generated almost entirely by the forelimbs (Schutt Jr. et al., 1997) instead of both the forelimbs and the hindlimbs in pterosaurs (Habib, 2008; Witton, 2013).

While the difference in the structural strength of pterosaur forelimb and hindlimb bones led to the original proposal of the quadrupedal take-off (Habib, 2008) and a recent study quantitatively investigated quadrupedal water take-off (Pittman et al., 2022), there has been very limited quantitative testing of the terrestrial take-off published (Padian et al., 2021; Griffin et al., 2022). Particularly of note, the ability of these take-off motions to generate the leverage that would be necessary to propel large pterosaurs into the air has not been quantitatively tested. One method for assessing leverage in extinct animals is the calculation of muscle moment arms (Hutchinson et al., 2005; Bates et al., 2012; Maidment, Bates & Barrett, 2014; Allen, Kilbourne & Hutchinson, 2021; Bishop, Cuff & Hutchinson, 2021). While muscle lines of action have been presented previously for pterosaurs (Fastnacht, 2005; Costa, Rocha-Barbosa & Kellner, 2014) these studies focussed primarily on myological reconstruction for terrestrial locomotion and did not calculate the moment arms.

To test the ability of different pterosaur take-off hypotheses to produce leverage during the launch phase we have constructed the first OpenSim musculoskeletal model pterosaur. This model is based on a 5 m wingspan ornithocheiraean pterosaur. Using this model, we have

why was this perim



estimated the take-off applicable muscle moment arms around each joint throughout the take-off motions for each of the hypothesised take-offs.

Materials & Methods

OpenSim modelling.

An ornithocheiraean musculoskeletal model was constructed using µCT scans of SMNK-PAL 1133, an indeterminate ornithocheiraean pterosaur. The OpenSim model was based upon a skeletal model made in Maya for a different study in 2015 (Martin-Silverstone, 2017; Martin-Silverstone, Sykes & Naish, 2018; Griffin et al., 2022). The surface meshes from the skeletal model were checked and any errors were cleaned using Geomagic Studio (3Dsystems, Morrisville, NC, USA). The articulated OpenSim model was constructed utilising the cleaned surface meshes and fitted geometric shapes following the workflow of Meilak *et al.* (Meilak et al., 2021a) using MATLAB v2021a, ParaView v5.9.0-RC3 (Ahrens, Geveci & Law, 2004), and OpenSim v4.0 and v4.1 (Seth et al., 2018). Due to the incomplete nature of SMNK-PAL 1133 scaled cylinders were added to represent the tibia and wing phalanges III and IV while duplicates of existing elements were used for missing vertebrae. The anterior skull is a scaled version of AMNH FARB 24444 combined with the anterior section of SMNK 1133 (Griffin et al., 2022).

Muscle Geometry.

Twenty-two muscles related to forelimb motion and a further twelve muscles related to the movement of the hip and knee joints were modelled as muscle tendon units (MTUs) in the OpenSim model following the estimated lines of action between the origin and insertion points (Table 1 including abbreviations, Figure 1). The MTUs were modelled based upon examination of physical specimens (Supplementary Material) and muscle reconstructions in the literature





122

123

124

125

126

127

128

129

130

131

132

133

134

135

136

137

138

139

140

141

142

143

144

(Dilkes, 1999; Bennett, 2001a,b, 2003, 2008; Fastnacht, 2005; Molnar, 2009; Witton, 2013; Costa, Rocha-Barbosa & Kellner, 2014; Tokita, 2015; Frigot, 2017). Inference levels for the presence of each muscle were determined following the extant phylogenetic bracket (EPB) inference model of Witmer (Witmer, 1995) and recorded in Table 1. Pterosaurs are bracketed by crocodiles and birds, following the most accepted interpretation of Pterosauromorpha as the sister-group of the Dinosauromorpha within Archosauria (Ezcurra et al., 2020; Baron, 2021; Foffa et al., 2022; Kellner et al., 2022). Muscles were only modelled when the inferred levels of confidence (as established by Witmer (Witmer, 1995)) for their origin and insertion were assessed as either I or II (positive or equivocal assessment, respectively). Whenever direct correlates in the form of osteological markers could not be identified, apostrophes (as in I' and II') indicate that correlates were missing, but reconstruction is still carried out based on the myological patterns present in the phylogenetic bracketing groups. Supplementary Table 1 summarizes all areas of origin and insertion, as well as their respective correlates (when present) and inference levels, for each reconstructed muscle. In the model, each origin and insertion point were placed at the centroids of the inferred areas of attachment with interpenetration between the bone meshes and the MTUs controlled by via points and wrapping surfaces (Hutchinson et al., 2015; Modenese & Kohout, 2020; Bishop, Cuff & Hutchinson, 2021; Meilak et al., 2021a; Wiseman et al., 2021).

To portray the complex lines of action more accurately in muscles with multiple origins such as the *m. triceps* and the *m. flexor tibialis internus* each muscle head was modelled individually (Table 1). For large muscles with broad attachment areas multiple lines of action were modelled at the cranial and caudal extents of the muscle in addition to a central muscle line of action. For the *m. pectoralis* lines of action were modelled at the cranial, caudal, medial, and lateral origin extent instead of a central muscle line of action, to better capture the broad



origin and insertion of the muscle. In total, the present model includes 36 MTUs pertaining to wing musculature, and 18 MTUs related to the hip and knee musculature (Table 1).

Kinematics.

Key poses from the literature (Bramwell & Whitfield, 1974; Padian, 1983; Fastnacht, 2005; Molnar, 2009; Chatterjee & Templin, 2012; Witton, 2013; Costa, Rocha-Barbosa & Kellner, 2014; Padian et al., 2021) for the hypothesised take-offs were created for the OpenSim model and corrected to fit within the range of motion calculated for the model via a previous study using the ROM mapping methodology (Griffin et al., 2022). Intermediate poses were extrapolated using inverse kinematics in Maya and OpenSim to create a full kinematic profile of each take-off (Figure 2). The timing between each pose was determined by relating the timing of each key pose of the model take-off sequences with the timing of the equivalent pose in the extant take-off sequences for the different take-off styles (Schutt Jr. et al., 1997; Earls, 2000). The total time of the entire model sequence was then normalised as one second take-off motions.

The bipedal burst take-off timings are based on a quail profile (Earls, 2000) and the description by Padian *et al.* (Padian et al., 2021). The take-off has been split into three phases (Figure 2A) starting with the crouch phase which begins in the fully crouched pose and lasts until the ankle joint loses contact with the ground. From this point the second phase, termed the ankle lifted phase, contains the continued leg extension, finishing when the pterosaur reaches a fully digitigrade pose. The final phase is the launch phase where the leg extension moves the pterosaur from the digitigrade pose to the point where the feet lose contact with the ground and the wing moves to the start of the flight downstroke position.

The bipedal countermotion timings are based on a starling profile (Earls, 2000) and the earlier descriptions of pterosaur bipedal take-off poses (Padian, 1983; Chatterjee & Templin,





2004, 2012; Fastnacht, 2005). The take-off has been split into two phases (Figure 2B). The first phase is termed the countermotion phase and contains the starting bipedal stance through the flexion of the hindlimb and the unfurling of the wing. The second phase is the launch phase and includes the extension of the hindlimb and movement of the wing into the start of the flight downstroke position.

The quadrupedal take-off timing is based on a vampire bat profile (Schutt Jr. et al., 1997) and primarily follows the description by Habib (Habib, 2008) modified by other descriptions of key poses in the literature (Fastnacht, 2005; Molnar, 2009; Witton, 2013). The quadrupedal take-off has been split into three phases (Figure 2C). The first phase is termed the crouch phase which begins in a quadrupedal stance pose and continues until the hindlimbs and forelimbs are fully flexed. The vault phase then includes the extension of the hindlimbs as the pterosaur pushes itself fully onto the forelimbs. The final phase is the launch, wherein the forelimbs extend until they leave the ground and the hindlimbs assume the pose that will be utilised in flight. As the bat profile timing largely ignored the hindlimbs the timing of the hindlimb leaving the ground in the vault phase was added using the timing of the literature descriptions of the pterosaur quadrupedal take-off (Habib, 2008; Molnar, 2009) relative to the timing of this phase for the forelimbs.

Moment Arm analysis.

Moment arms were recorded for each pose throughout the take-off kinematics in the shoulder, elbow, wrist, wing metacarpal, and wing phalanx 1 in the forelimb and the hip and the knee in the hindlimb. These joints were selected as they are the joints proposed to be utilised in the different launch hypotheses. The ankle joint was not included due to the lack of an accurate bone models of the tibia and metatarsals, preventing accurate mapping of the MTUs. Moment arms were calculated and exported using the plotting tool in OpenSim for the kinematic sequence of each take-off in each joint degree of freedom (DOF). OpenSim calculates moment



arms using the in-built the virtual work methodology (An et al., 1984; Pandy, 1999; Delp & Loan, 2000; Sherman, Seth & Delp, 2013). Exported moment arms were then analysed using a modified R script (R version 4.1.2, Rstudio version 2021.09.2+382) based upon the methodology of Wiseman et al. (Wiseman et al., 2021). As in the Wiseman methodology a Monte Carlo simulation of each muscle moment arm value was run wherein the value was independently allowed to uniformly randomise by values of up to ± 20% for 1000 simulated trials in order to create error margins accounting for errors in moment arm estimation. The resultant distribution was then analysed for both the mean moment arm and the standard deviation. The mean moment arms for each muscle were collated to determine the total summed moment arms and overall direction of the moment arm acting upon the joint at each point in the launch hypothesis motions.

Results

The following results apply the summed directional moment arms and associated estimation error calculated from the Monte Carlo approach plotted against the launch kinematics (Figures 3-5). Trends applicable to launch are summarised below.

Bipedal Burst.

The hip abductors through the bipedal burst kinematic initially decrease before plateauing in the ankle lifted phase of the take-off. The adductors show a steady increase through the entire kinematic. With regards to rotation the internal rotators of the hip decrease through the entire take-off sequence while the extensors only begin to increase noticeably during the ankle lifted phase. The flexor moment arms in the hip slightly increase through the entire take-off kinematic as do the hip and knee extensors. The knee flexors also sharply increase during the crouched phase before beginning to slow during the ankle lifted phase.



Bipedal Countermotion.

For the bipedal countermotion kinematic the moment arms of the hip abductors show an increase through the countermotion before decreasing in the launch phase. The adductors show a slight decrease during the countermotion phase, increase slightly at the start of the launch phase before ultimately decreasing further. Regarding hip rotational moment arms the internal rotators are largely unchanged through the countermotion phase and then increase slightly during the launch phase. The external rotator moment arms decrease throughout the countermotion phase and then increase through the launch phase. For the flexor moment arms there is a decrease through the countermotion phase and in increase through the launch phase. This pattern is repeated in the hip extensor moment arms until midway through the launch phase where the length of the moment arms begins to decrease again. The knee flexor moment arms increase through the countermotion phase and decrease through the launch phase while the knee extensor moment arms remain largely unchanged throughout the take-off kinematic.

Quadrupedal.

Shoulder abductors through the quadrupedal take-off kinematic remain largely equivalent until the launch phase where they see a decrease in leverage, conversely the hip abductors increase until the hindlimbs leave the ground in the vault phase. The shoulder adductors show an increasing trend until the launch phase where it sharply decreases while the hip adductors decrease until the vault phase. The shoulder internal rotation DOF moment arms increase through the crouch phase and decrease through the rest of the take-off kinematic while the external rotation DOF shows the reverse. The hip internal rotators feature a decrease in the middle of the crouch phase but are otherwise largely unchanged. The external rotators on the other hand feature a pronounced decrease through the crouch phase.



The shoulder flexion moment arms decrease through the crouch phase before increasing slowly in the vault and rapidly in the launch phase. The extensor moment arms slightly increase throughout the kinematic until the launch phase where they rapidly decrease. The elbow flexors slightly decrease through the crouch phase. This decrease becomes more pronounced in the vault phase and reverses in the launch phase. The extensor moment arms slightly increase throughout the crouch and vault phases before decreasing during the launch phase. The wrist flexion moment arms increase during the crouch phase and then decrease through the rest of the take-off while the extensor moment arms are largely unchanged through the kinematic sequence. The wing metacarpal (WMC) moment arm trends are equivalent to the trends in the wrist however the WMC extension moment arms are half a large as the equivalent wrist moment arms. The moment arms of the first wing phalanx (WP1) flexors are largely consistent through the crouch phase before dipping slightly in the later phases of the take-off. The extensors decrease until the end of the crouch phase and then increase again. In the hindlimb, the hip flexors and extensors along with the knee extensors decrease through the crouch phase while the knee flexors increase.

Discussion

The largest moment arms that occur for each of the simulated take-offs occurs in the upper forelimb joints, specifically in the elbow flexion/extension DOF and the shoulder abduction/adduction DOF (Figure 3). The largest moment arms in the hindlimbs occur in each of the hip DOFs and are largely equivalent between the different launches; except for the hip external rotation DOF which has a smaller moment arm during the burst take-off (Figure 5). Overall, the largest hindlimb moment arm is half the length of the largest forelimb moment arm. The smallest moment arms occur in the extensional DOF of WP1 in the lower forelimb (Figure 4).



265

266

267

268

269

270

271

272

273

274

275

276

277

278

279

280

281

282

283

284

285

286

287

The largest summed moment arms are recorded in the forelimb for all three take-off hypotheses, with the largest moment arms occurring in the quadrupedal take-off profile. Trends within the take-off moment arms closely match phase changes within the different take-off kinematics in all but the burst take-off hindlimb DOFs (Figure 5). There is distinct overlap in the forelimb DOFs for the bipedal take-off motions which correspond with the wings gaining sufficient clearance to fully open without striking the ground. Similarly, both the bipedal countermotion and quadrupedal take-off hindlimb DOFs strongly overlap during the countermotion phases of each take-off kinematic before diverging during the later phases. The peak moment arms for the bipedal burst take-off tend to occur at launch or at the start of the take-off sequence. The peak moment arms of the bipedal countermotion take-off tend to occur during the countermotion phase or at launch except for the hip abduction and extension degrees of freedom where the peak occurs at the start of the sequence. The quadrupedal take-off peak moment arms occur at launch or the end of the crouch phase in the forelimb and at the end of the crouch phase or start of the take-off sequence in the hindlimb, except for the hip long axis rotation peak which occurs at launch as the hindlimbs assume the flight pose. Overall, when all of the moment arms are considered, the quadrupedal take-off summed moment arms are greater in magnitude than moment arms associated with the other two take-offs scenarios.

It must also be noted that despite including the moment arms of the forelimbs in the bipedal take-off models, forelimbs would not be utilised at the point of take-off. In both bipedal take-offs the forelimbs are not used until the initial downstroke of the wings by which time launch has already occurred (Padian, 1983; Padian et al., 2021). Similarly, the quadrupedal take-off does not utilise the hindlimb moment arms at the point of launch. The quadrupedal take-off only utilises the hindlimbs until they lose contact with the ground during the vault phase of the take-off (Habib, 2008).



A complication in the muscular reconstruction process are the prominent differences between crocodilian and avian estimations in the presence or absence of different muscles. The TM, HR, FDL.U, and TR.M are absent in birds, and the TR.C is variable between species but are all present in crocodilians; conversely the FCR is not present in crocodilians (Dilkes, 1999; Bennett, 2003, 2008). The inclusion of these muscles results in changes to the muscle reconstruction and the resultant moment arms of the model with entirely avian based moment arms being slightly reduced compared to purely crocodilian or combined models (See Supplementary). While it is possible to determine the presence of some muscles via muscle scars left on the fossils it is important for the inferences to be clear for the results of any modelling attempts.

While the ankle joint would be utilised at some stage in all the hypothesised take-offs, our model was not able to reconstruct this joint with precision due to the missing model bones in the reference specimen. Attempting muscle reconstruction without accurate models of the missing bones would result in substantial error from uncertainty in the origin and insertion points of the muscles (Meilak et al., 2021a). Other studies that have examined the moments produced around the ankle in crocodilians and birds (Meilak et al., 2021a,b; Wiseman et al., 2021). As both crocodilians and pterosaurs are plantigrade (Mazin et al., 2003; Mazin & Pouech, 2020), and lack the tibiotarsus seen in birds, a crocodilian ankle mechanics approach may be a closer approximation if the ankle muscles were to be estimated. These studies found the moments produced by crocodiles to peak at be around half the peak moment of the knee (Wiseman et al., 2021) while birds tended to peak at moment values equal or greater than the knee (Meilak et al., 2021a,b). If such results are applied to pterosaurs it is unlikely for either of the bipedal take-off motions reach an equivalent amount of leverage as the quadrupedal launch motion.

When proposing a quadrupedal take-off, Habib (Habib, 2008) determined that the forelimbs of pterosaurs are stronger than the hindlimbs and as a result were likely able to



314

315

316

317

318

319

320

321

322

323

324

325

326

327

328

329

330

331

332

333

334

335

336

337

338

withstand loads associated with quadrupedal launch. Our results further support this finding by determining that the muscle moment arms of the forelimb would be able to exert are also larger than the hindlimb, allowing pterosaurs to utilise the greater force resistance highlighted by Habib. Our own prior research into pterosaur range of motion found that ornithocheiraean pterosaurs can assume the poses required to quadrupedally take-off even when constrained by soft tissues (Griffin et al., 2022). The OpenSim model results indirectly lend support to the water take-off findings of Pittman et al. (Pittman et al., 2022) by highlighting the leverage possible in both the fore and hindlimbs which could be used to power water take-offs. These results are contrary to the findings presented by Padian et al., (Padian et al., 2021) however that study focuses on a different pterosaur morphology, that of the giant azhdarchids. This previous study also highlighted the lack of moment arm analyses for the different launch hypotheses and raised concerns regarding the use of bats as models for quadrupedal take-offs due to the lack of hindlimb use by bats. This study addresses the moment arm concerns by determining that the moment arms of three different pterosaur take-off kinematics and found the launch leverage available through via quadrupedal take-off (Figure 4) and for the quadrupedal take-off pose to be the largest of the launch scenarios. Due to the lack of other recorded quadrupedally launching modern fliers from which to compare and derive timings, bat-based timing for the modelling of take-off in pterosaurs remains unavoidable though we have also incorporated hindlimb kinematics into the pterosaur take-off models. Future work may be able to refine the kinematics and better address this concern, potentially through forward kinematic approaches or iterative optimisation of reverse kinematic approaches (Bishop et al., 2021). Further work is also needed to apply muscular force estimations to the moment arms calculated for the pterosaur model as leverage does not automatically translate to increase force transfer. Additionally, the methods utilised in this study also need to be applied to the azhdarchid and non-pterodactyloid pterosaur morphologies to better facilitate comparison and develop a more complete understanding of pterosaur take-off.







Acknowledgements

The authors would like to acknowledge the μ -VIS X-ray Imaging Centre at the University of Southampton for provision of tomographic imaging facilities.

Competing Interests

We have no conflicts of interest to declare.

Author Contributions

All authors contributed to writing the manuscript. BG co-designed the study, collected the data, created the models, and ran the analyses. EMS co-designed the study, supplied the original fossil material scans, sense-checked the soft tissue reconstructions and supervised the project. EM created the OpenSim model creation pipeline and assisted with model creation. RP sense-checked the soft tissue reconstructions. FC sense-checked the soft tissue reconstructions. CP co-designed the study and supervised the project. ER co-designed the study and supervised the project.

PeerJ

354	References
355 356	Ahrens J, Geveci B, Law C. 2004. ParaView: an End-UserTool for Large Data Visualization. In: Hansen CD, Johnson CR eds. <i>Visualisation Handbook</i> . Elsevier,.
357 358	Alexander RM. 1998. All-time giants: the largest animals and their problems. <i>Palaeontology</i> 41:1231–1245.
359 360	Allen VR, Kilbourne BM, Hutchinson JR. 2021. The evolution of pelvic limb muscle moment arms in bird-line archosaurs. <i>Science Advances</i> 7. DOI: 10.1126/sciadv.abe2778.
361 362 363	An KN, Takahashi K, Harrigan TP, Chao EY. 1984. Determination of muscle orientations and moment arms. <i>Journal of Biomechanical Engineering</i> 106:280–282. DOI: 10.1115/1.3138494.
364 365	Baron MG. 2021. The origin of Pterosaurs. <i>Earth-Science Reviews</i> 221. DOI: 10.1016/j.earscirev.2021.103777.
366 367 368 369	Bates KT, Maidment SCR, Allen VR, Barrett PM. 2012. Computational modelling of locomotor muscle moment arms in the basal dinosaur <i>Lesothosaurus diagnosticus</i> : Assessing convergence between birds and basal ornithischians. <i>Journal of Anatomy</i> 220:212–232. DOI: 10.1111/j.1469-7580.2011.01469.x.
370 371 372	Bennett SC. 2001a. The Osteology and Functional Morphology of the Late Cretaceous Pterosaur <i>Pteranodon</i> Part II. Size and Functional Morphology. <i>Palaeontographica, Abteilung A: Palaozoologie - Stratigraphie</i> 260:113–153.
373 374 375	Bennett SC. 2001b. The Osteology and Functional Morphology of the Late Cretaceous Pterosaur <i>Pteranodon</i> : Part I. General Description of Osteology. <i>Palaeontographica, Abteilung A: Palaozoologie - Stratigraphie</i> 260:113–153.
376 377 378	Bennett SC. 2003. Morphological evolution of the pectoral girdle of pterosaurs: myology and function. <i>Geological Society, London, Special Publications</i> 217:191–215. DOI: 10.1144/GSL.SP.2003.217.01.12.
379 380 381	Bennett SC. 2008. Morphological evolution of the wing of pterosaurs: Myology and function. Zitteliana Reihe B: Abhandlungen der Bayerischen Staatssammlung fur Palaontologie und Geologie:127–141.
382 383 384	Bishop PJ, Cuff AR, Hutchinson JR. 2021. How to build a dinosaur: Musculoskeletal modeling and simulation of locomotor biomechanics in extinct animals. <i>Paleobiology</i> 47:1–38. DOI: 10.1017/pab.2020.46.
385 386 387	Bishop PJ, Falisse A, De Groote F, Hutchinson JR. 2021. Predictive Simulations of Musculoskeletal Function and Jumping Performance in a Generalized Bird. <i>Integrative Organismal Biology</i> 3. DOI: 10.1093/iob/obab006.
388 389	Bramwell CD, Whitfield GR. 1974. Biomechanics of <i>Pteranodon</i> . <i>Philosophical Transactions of the Royal Society B: Biological Science</i> 267:503–581.
390 391 392	Chatterjee S, Templin RJ. 2004. Posture, locomotion, and paleoecology of pterosaurs. Geological Society of America Special Publication 376:1–64. DOI: 10.1130/0-8137-2376-0.1.



393	Chatterjee S, Templin RJ. 2012. The Flight Dynamics of <i>Tapejara</i> , a Pterosaur From the Early
394	Cretaceous of Brazil with a Large Cranial Crest. Acta Geologica Sinica - English Edition
395	86:1377–1388. DOI: 10.1007/s00192-011-1546-5.

- Costa FR, Rocha-Barbosa O, Kellner AWA. 2014. Myological reconstruction of the pelvic girdle of *Anhanguera piscator* (Pterosauria: Pterodactyloidea) using three dimensional virtual animation. *Revista Brasileira de Paleontologia* 17:11–22. DOI: 10.4072/rbp.2014.1.02.
- Delp SL, Loan JP. 2000. A computational framework for simulating and analyzing human and animal movement. *Computing in Science and Engineering* 2. DOI: 10.1109/5992.877394.
- Dilkes DW. 1999. Appendicular myology of the hadrosaurian dinosaur *Maiasaura peeblesorum* from the Late Cretaceous (Campanian) of Montana. *Transactions of the Royal Society of Edinburgh: Earth Sciences* 90:87–125. DOI: 10.1017/S0263593300007185.
- Earls K. 2000. Kinematics and Mechanisms of Ground Take-off in the Startling *Sturnis Vulgaris* and the Quail *Coturnix Coturnix*. *Journal of Experimental Biology* 203:725–739. DOI: 10.1523/JNEUROSCI.2773-10.2010.
- Ezcurra MD, Nesbitt SJ, Bronzati M, Dalla Vecchia FM, Agnolin FL, Benson RBJ, Brissón Egli F, Cabreira SF, Evers SW, Gentil AR, Irmis RB, Martinelli AG, Novas FE, Roberto da Silva L, Smith ND, Stocker MR, Turner AH, Langer MC. 2020. Enigmatic dinosaur precursors bridge the gap to the origin of Pterosauria. *Nature* 588:445–449. DOI: 10.1038/s41586-020-3011-4.
- Fastnacht M. 2005. The first dsungaripterid pterosaur from the Kimmeridgian of Germany and the biomechanics of pterosaur long bones. *Acta Palaeontologica Polonica* 50:273–288.
- Foffa D, Dunne EM, Nesbitt SJ, Butler RJ, Fraser NC, Brusatte SL, Farnsworth A, Lunt DJ, Valdes PJ, Walsh S, Barrett PM. 2022. *Scleromochlus* and the early evolution of Pterosauromorpha. *Nature* 610:313–318. DOI: 10.1038/s41586-022-05284-x.
- Frigot RA. 2017. Pelvic musculature of *Vectidraco daisymorrisae* and consequences for pterosaur locomotion. *Geological Society of London Special Publication* 455:45–55. DOI: 10.1016/j.matlet.2011.05.028.
- Goto Y, Yoda K, Weimerskirch H, Sato K. 2022. How did extinct giant birds and pterosaurs fly?

 A comprehensive modeling approach to evaluate soaring performance. *PNAS Nexus*:1–16.

 DOI: 10.1093/pnasnexus/pgac023.
- Griffin B, Martin-Silverstone E, Demuth O, Pêgas R, Palmer C, Rayfield E. 2022. Constraining pterosaur launch: range of motion in the pectoral and pelvic girdles of a medium-sized ornithocheiraean pterosaur. *Biological Journal of the Linnean Society*. DOI: 10.1093/biolinnean/blac063.
- Habib MB. 2008. Comparative evidence for quadrupedal launch in pterosaurs. *Zitteliana* B28:159–166.
- Henderson DM. 2010. Pterosaur body mass estimates from three-dimensional mathematical slicing. *Journal of Vertebrate Paleontology* 30:768–785. DOI:
- 431 10.1080/02724631003758334.

432 433 434	aeronautical function and ecological implications. <i>Palaeogeography, Palaeoclimatology, Palaeoecology</i> 440:431–439. DOI: 10.1016/j.palaeo.2015.08.046.
435 436 437 438	Hutchinson JR, Anderson FC, Blemker SS, Delp SL. 2005. Paleontological Society Analysis of Hindlimb Muscle Moment Arms in <i>Tyrannosaurus rex</i> Using a Three- Dimensional Musculoskeletal Computer Model: Implications for Stance, Gait, and Speed Author (s): John R. Hutchinson, Frank C. Anderson, Silvia S. <i>Paleobiology</i> 31:676–701.
439 440 441 442	Hutchinson JR, Rankin JW, Rubenson J, Rosenbluth KH, Siston RA, Delp SL. 2015. Musculoskeletal modelling of an ostrich (<i>Struthio camelus</i>) pelvic limb: Influence of limb orientation onmuscular capacity during locomotion. <i>PeerJ</i> 2015:1–52. DOI: 10.7717/peerj.1001.
443 444 445 446	Kellner AWA, Holgado B, Grillo O, Pretto FA, Kerber L, Pinheiro FL, Soares MB, Schultz CL, Lopes RT, Araújo O, Müller RT. 2022. Reassessment of <i>Faxinalipterus minimus</i> , a purported Triassic pterosaur from southern Brazil with the description of a new taxon. <i>PeerJ</i> 10. DOI: 10.7717/peerj.13276.
447 448	Maidment SCR, Bates KT, Barrett PM. 2014. Modeling of pelvic locomotor muscle moment arms in <i>Edmontosaurus</i> . <i>Hadrosaurs</i> .
449 450	Martin-Silverstone E. 2017. Insights into mass estimation, pneumaticity, and anatomy of pterosaurs: implications for locomotion. University of Southampton.
451 452 453 454	Martin-Silverstone E, Sykes D, Naish D. 2018. Does postcranial palaeoneurology provide insight into pterosaur behaviour and lifestyle? New data from the azhdarchoid <i>Vectidraco</i> and the ornithocheirids <i>Coloborhynchus</i> and <i>Anhanguera</i> . <i>Palaeontology</i> 62:197–210. DOI: 10.1111/pala.12390.
455 456 457	Mazin JM, Billon-Bruyat J-P, Hantzepergue P, Larauire G. 2003. Ichnological evidence for quadrupedal locomotion in pterodactyloid pterosaurs: Trackways from the Late Jurassic of Crayssac. In: <i>Evolution and Palaeobiology of Pterosaurs</i> . 283–296.
458 459 460	Mazin JM, Pouech J. 2020. The first non-pterodactyloid pterosaurian trackways and the terrestrial ability of non-pterodactyloid pterosaurs. <i>Geobios</i> 58:39–53. DOI: 10.1016/j.geobios.2019.12.002.
461 462 463	Meilak EA, Gostling NJ, Palmer C, Heller MO. 2021a. On the 3D Nature of the Magpie (Aves: Pica pica) Functional Hindlimb Anatomy During the Take-Off Jump. <i>Frontiers in Bioengineering and Biotechnology</i> 9. DOI: 10.3389/fbioe.2021.676894.
464 465	Meilak EA, Provini P, Palmer C, Gostling NJ, Heller MO. 2021b. On the hindlimb biomechanics of the avian take-off leap. <i>bioRxiv preprint</i> . DOI: 10.1101/2021.11.19.469279.
466 467 468	Modenese L, Kohout J. 2020. Automated Generation of Three-Dimensional Complex Muscle Geometries for Use in Personalised Musculoskeletal Models. <i>Annals of Biomedical Engineering</i> 48:1793–1804. DOI: 10.1007/s10439-020-02490-4.
469 470	Molnar J. 2009. How giant reptiles flew: visualizing quadrupedal launch in pterosaurs. Johns Hopkins University.



471	Padian K. 1983. A Functional Analysis of Flying and Walking in Pterosaurs. Paleobiology
472	9:218–239. DOI: 10.1042/BST20150065.

- Padian K, Cunningham JR, Langston W, Conway J. 2021. Functional morphology of
- 474 *Quetzalcoatlus* Lawson 1975 (Pterodactyloidea: Azhdarchoidea). *Journal of Vertebrate*
- 475 Paleontology 41:218–251. DOI: 10.1080/02724634.2020.1780247.
- Pandy MG. 1999. Moment Arm of a Muscle Force. *Exercise and Sport Science Reviews* 27:79–118.
- Pennycuick CJ. 1968. Power requirements for horizontal flight in the pigeon *Columba livia*. Journal of Experimental Biology 49:527–555.
- Pittman M, Kaye TG, Campos HBN, Habib MB. 2022. Quadrupedal water launch capability
- demonstrated in small Late Jurassic pterosaurs. Scientific Reports 12:1–8. DOI:
- 482 10.1038/s41598-022-10507-2.
- 483 Rayner JM V. 1988. Form and Function in Avian Flight. *Current Ornithology* 5:1–66. DOI: 10.1007/978-1-4615-6787-5_1.
- Rayner JM V. 1989. Mechanics and physiology of flight in fossil vertebrates. *Transactions of the Royal Society of Edinburgh: Earth Sciences* 80:311–320.
- Schutt Jr. WA, Scott Altenbach J, Chang YHH, Cullinane DMM, Hermanson JW, Muradali F, Bertram JEAE. 1997. The dynamics of flight-initiating jumps in the common vampire bat
- Desmodus rotundus. The Journal of experimental biology 200:3003–12. DOI: citeulike-
- 490 article-id:418833.
- Seth A, Hicks JL, Uchida TK, Habib A, Dembia CL, Dunne JJ, Ong CF, DeMers MS, Rajagopal
- 492 A, Millard M, Hamner SR, Arnold EM, Yong JR, Lakshmikanth SK, Sherman MA, Ku JP,
- 493 Delp SL. 2018. OpenSim: Simulating musculoskeletal dynamics and neuromuscular control
- to study human and animal movement. *PLOS Computational Biology* 14:e1006223. DOI:
- 495 10.1371/journal.pcbi.1006223.
- Sherman MA, Seth A, Delp SL. 2013. What is a moment arm? Calculating muscle effectiveness
- in biomechanical models using generalized coordinates. In: *Proceedings of the ASME*
- 498 2013 International Design Engineering Technical Conferences and Computers and
- 499 Information in Engineering Conference. 1–9.
- Tokita M. 2015. How the pterosaur got its wings. *Biological Reviews* 90:1163–1178. DOI: 10.1111/brv.12150.
- Wiseman ALA, Bishop PJ, Demuth OE, Cuff AR, Michel KB, Hutchinson JR. 2021.
- 503 Musculoskeletal modelling of the Nile crocodile (*Crocodylus niloticus*) hindlimb: Effects of
- limb posture on leverage during terrestrial locomotion. *Journal of Anatomy* 239:424–444.
- 505 DOI: 10.1111/joa.13431.
- 506 Witmer LM. 1995. The Extant Phylogenetic Bracket and the importance of reconstructing soft
- 507 tissues in fossils. In: Thompson J ed. Functional Morphology in Vertebrate Paleontology.
- New York, New York: Cambridge University Press, 19–33.





509 510	Witton MP. 2008. A new approach to determining pterosaur body mass and its implications for pterosaur flight. <i>Zitteliana</i> B28:143–159.
511 512	Witton MP. 2013. <i>Pterosaurs Natural History, Evolution, Anatomy</i> . Princeton, USA: Princeton University Press.
513 514 515	Witton MP, Habib MB. 2010. On the size and flight diversity of giant pterosaurs, the use of birds as pterosaur analogues and comments on pterosaur flightlessness. <i>PLoS ONE</i> 5:e13982. DOI: 10.1371/journal.pone.0013982.
516	
517	
518	Software References
519	Geomagic Studio, 3Dsystems, Morrisville, NC, USA.
520	MATLAB version 2021a. Mathworks Inc., URL: uk.mathworks.com/products/matlab
521	Maya 2019. Autodesk, URL: www.autodesk.co.uk/products/maya
522	ParaView version 5.9.0-RC3. Kitware, URL: www.paraview.org
523	R Core Team (2021). R: A language and environment for statistical computing. R Foundation for
524	Statistical Computing, Vienna, Austria. Version 4.1.2 URL https://www.R-project.org/.

Table 1: Modelled muscle tendon units (MTUs) for the OpenSim Ornithocheiraean model. * indicates MTUs not directly related to the take-offs.

code	Muscle	Origin	Inference	Insertion	Inferenc e
		Pectoral group			
SCM*	sternocleidomastoideus	anterior sternum	1	squamosal	ľ
SC*	sternocoracoideus	anterior margin of sternum	II'	coracoid	II
LD	latissimus dorsi	last cervical neural spine to distal notarium – 3 MTUs	l'	dorsal (distal) humerus shaft scar	I
TM	teres major	posterolateral scapula	II	dorsal (proximal) humerus shaft scar	II
DS	deltoides scapularis	lateral scapula/acromion process	1	dorsal (anterior) deltopectoral crest	l'
SHA	scapulohumeralis anterior	scapula anterior to glenoid	II	dorsal (proximal) deltopectoral crest	11'
SHP	scapulohumeralis posterior	posterior margin scapula above glenoid	I	dorsal posterior process of humerus distal to SUBS	I
SUB S	subscapularis	medial ventral surface scapula	I	dorsal posterior process of humerus	I
TR-S	triceps	scapula - dorsal border of glenoid	I	olecranon process ulna	ı
TR-C	triceps	coracoid - ventral posterior to glenoid	11'	olecranon process ulna	II
TR-M	triceps	medial - posterior side humeral shaft	I	olecranon process ulna	I
TR-L	triceps	lateral - anterior side humeral shaft	II	olecranon process ulna	II
PECT	Pectoralis	sternum ventral – 4 MTUs	I	entire ventral deltopectoral crest	I
SUP C	supracoracoideus	anterior ventral surface of coracoid	II	ventral proximal to deltopectoral crest	II'
СВ	Coracobrachialis	posterior ventral coracoid – 3 MTUs	I	ventral posterior to deltopectoral crest	I
BI	Biceps	coracoid biceps tubercule	I	proximal radius/ulna – 2 MTUs	I
BR	brachialis	anterior humerus shaft	<u>'</u>	proximal radius/ulna	I
HR	humeroradialis	proximal humerus distal to CB	II'	proximal radius	II'
FDL	flexor digitorum longus (quarti)	medial epicondyle of humerus and ulna	II	ventral extensor process WP1 and distal phalanges	l'
FDL- U	flexor digitorum longus (quarti)	medial ulna shaft Ulna	I	ventral extensor process WP1 and distal phalanges	l'
EDL	extensor digitorum longus (quarti)	lateral epicondyle of humerus	I	proximal posterior WP1 process	l'
FCU	flexor carpi ulnaris	medial epicondyle of humerus	I	anterior proximal WMC	II'
FCR	flexor carpi radialis	medial epicondyle of humerus	I	Proximal anterior syncarpal	II
ECU	extensor carpi ulnaris	lateral epicondyle of humerus	1	posterior WMC large scar	II
ECR	extensor carpi radialis	lateral epicondyle of humerus	I	Proximal posterior syncarpal	II'
SUP	supinator	ridge anterior to lateral epicondyle of humerus	I	3/4 length of posterior radius shaft	I
PT	pronator teres	medial epicondyle of humerus	I	posterior mid shaft	1
PQ	pronator quadratus	ulna shaft	1	posterior distal radius shaft	1
FDB	flexor digitorum brevis	dorsal distal syncarpal	ll'	dorsal extensor process WP1	I

PeerJ

EDB	extensor digitorum brevis	ventral distal syncarpal	ll'	posterior WP1 process	II
		Pelvic Group			
ADD	adductor femoris	lateral surface of the ischium	1	medial shaft (diaphysis) of the femur	I
IFM	illiofemoralis	Lateral margin of preacetabular process of the ilium	I	greater trochanter	I
PIFE	puboischiofemoralis externus	Lateral surface of the pubis	I	greater trochanter	I
PIFI	puboischiofemoralis internus	medial surface of ilium anterior to acetabulum	I	proximal surface of femur	I
AMB	ambiens	pubic tubercule	I	cnemial crest of tibia	l'
ITB	Iliotibialis	Lateral margin of preacetabular process of the ilium – 3 MTUs	I	cnemial crest of tibia	ľ
FTE	flexor tibialis externus	lateral surface of the postacetabular process of the ilium	II	medial surface of the tibia	II'
FTI-I	flexor tibialis internus	lateral surface of ischial tuberosity – 2 MTUs	II	posteromedial shaft of tibia	II'
FTI-II	flexor tibialis internus 2	lateral surface of the postacetabular process of the ilium	II	posteromedial shaft of tibia	II'
ILF	iliofibularis	lateral surface of the postacetabular process of the ilium	ll'	posteromedial shaft of tibia	II'
CFB	caudofemoralis brevis	lateral iliac surface	l'	posterior (4th) trochanter of femur	I
FMTE	femorotibialis externus	proximal femoral shaft	I	cnemial crest of tibia	l'
FMTI	femorotibialis internus	proximal femoral shaft	1	cnemial crest of tibia	ľ





528	Figure captions:
529	Figure 1: Musculoskeletal model used in this study with labelled MTUs and joints in A) lateral, B)
530	posterior and C) anterior views. Muscle abbreviations follow the codes set forth in Table 1.
531	Figure 2: One second take-off sequences used in this study highlighting key phases. A) Bipedal
532	burst style take-off with crouched, ankle lifted, and launch phase timings highlighted. B) Bipedal
533	countermotion style take-off with countermotion and launch phase timings highlighted. C)
534	Quadrupedal take-off style with crouch, vault, and launch phases highlighted.
535	
536	Figure 3: Summed moment arms in each hypothesised take-off motion for the shoulder and
537	elbow rotational DOFs. Solid lines indicate mean values following Monte Carlo simulation,
538	dashed lines show estimated error, colouration indicates moment arm usage throughout the
539	take-off. Take-off phase markers are equivalent to Figure 2.
540	
541	Figure 4: Summed moment arms in each hypothesised take-off motion for the lower forelimb
542	rotational DOFs. Solid lines indicate mean values following Monte Carlo simulation, dashed
543	lines show estimated error, colouration indicates moment arm usage throughout the take-off.
544	Take-off phase markers are equivalent to Figure 2.
545	
546	Figure 5: Summed moment arms in each hypothesised take-off motion for the hindlimb
547	rotational DOFs. Solid lines indicate mean values following Monte Carlo simulation, dashed
548	lines show estimated error, colouration indicates moment arm usage throughout the take-off.
549	Take-off phase markers are equivalent to Figure 2.
550	







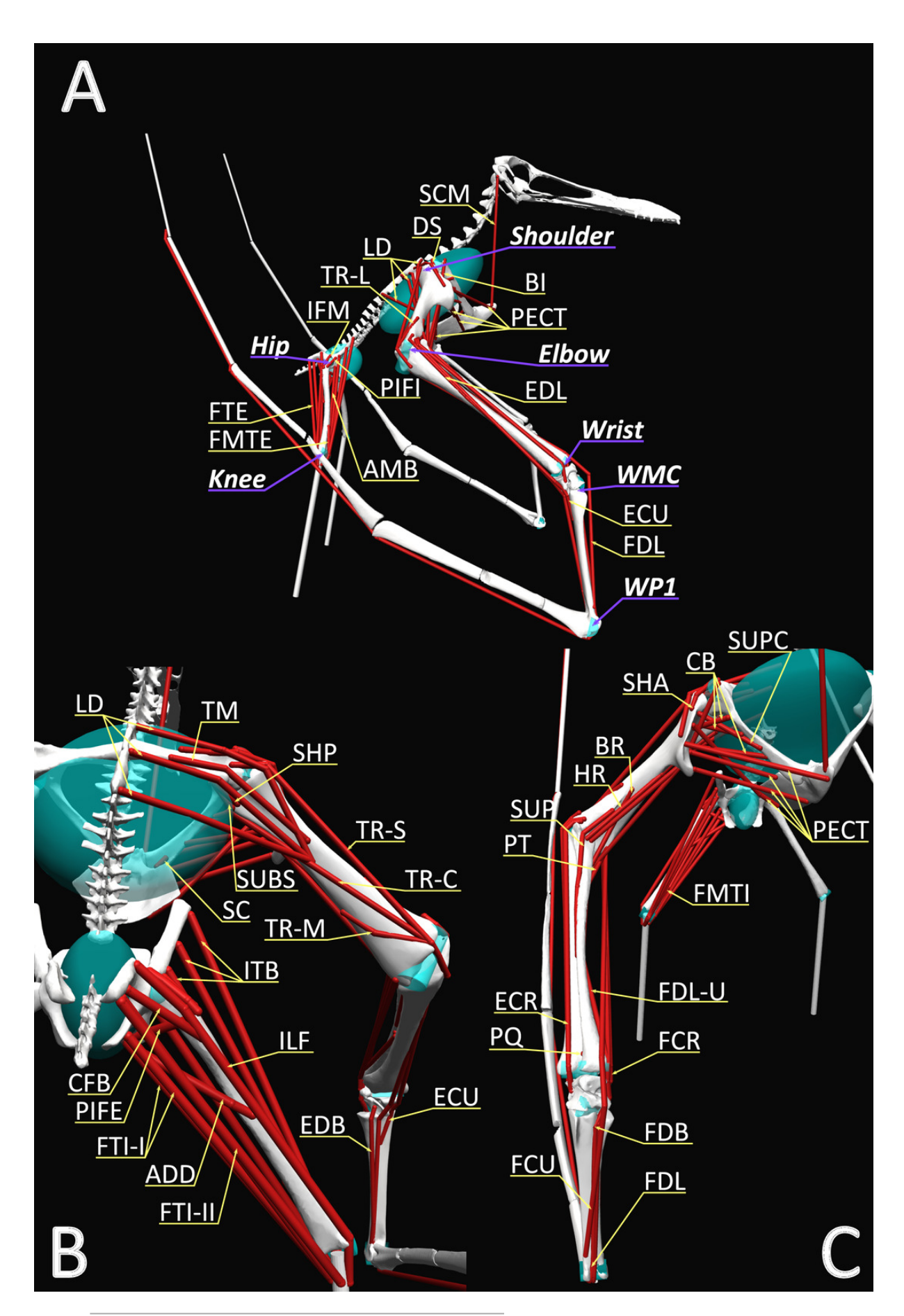


552	Supplementary summary:
553	Supplemental tables and figures included in separate document.
554	Supplemental Excel Workbook: Extended muscle reconstruction workbook available upon
555	request and will be uploaded to data.bris online repository (with DOI) on final publication.
556	Zip folder "MMA" contains all raw output data from OpenSim and subsequent randomisations.
557	This will also be included in the data.bris DOI.
558	Model Availability: 3D models of some of the skeletal elements are associated with previous
559	papers (Martin-Silverstone, Sykes & Naish, 2018; Griffin et al., 2022). The complete OpenSim
560	model and movement files will be uploaded to the data.bris repository and the OpenSim website
561	where it will be freely available to download on publication.



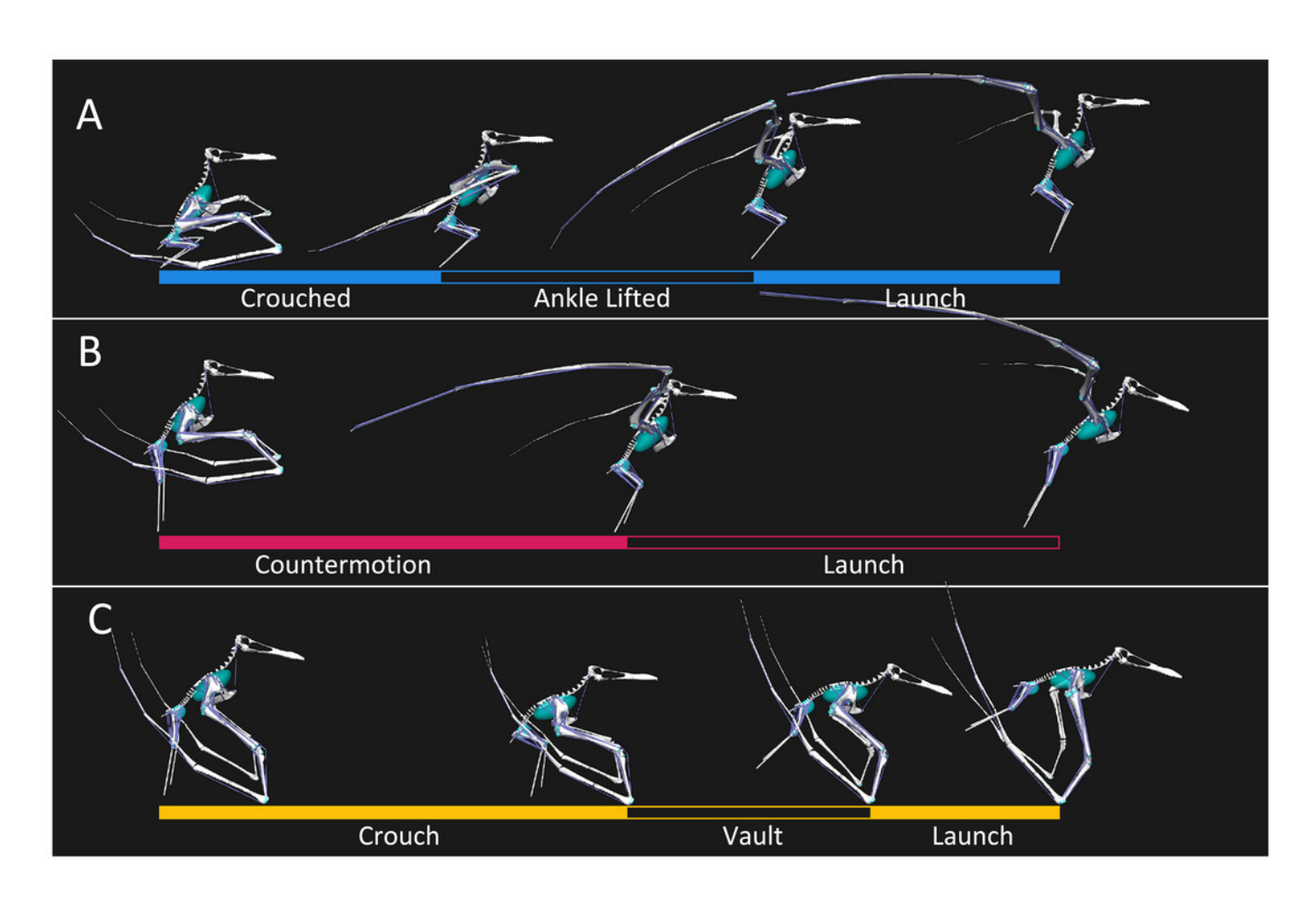
Musculoskeletal model used in this study with labelled MTUs and joints in A) lateral, B) posterior and C) anterior views.

Muscle abbreviations follow the codes set forth in Table 1.



One second take-off sequences used in this study highlighting key phases.

A) Bipedal burst style take-off with crouched, ankle lifted, and launch phase timings highlighted. B) Bipedal countermotion style take-off with countermotion and launch phase timings highlighted. C) Quadrupedal take-off style with crouch, vault, and launch phases highlighted.

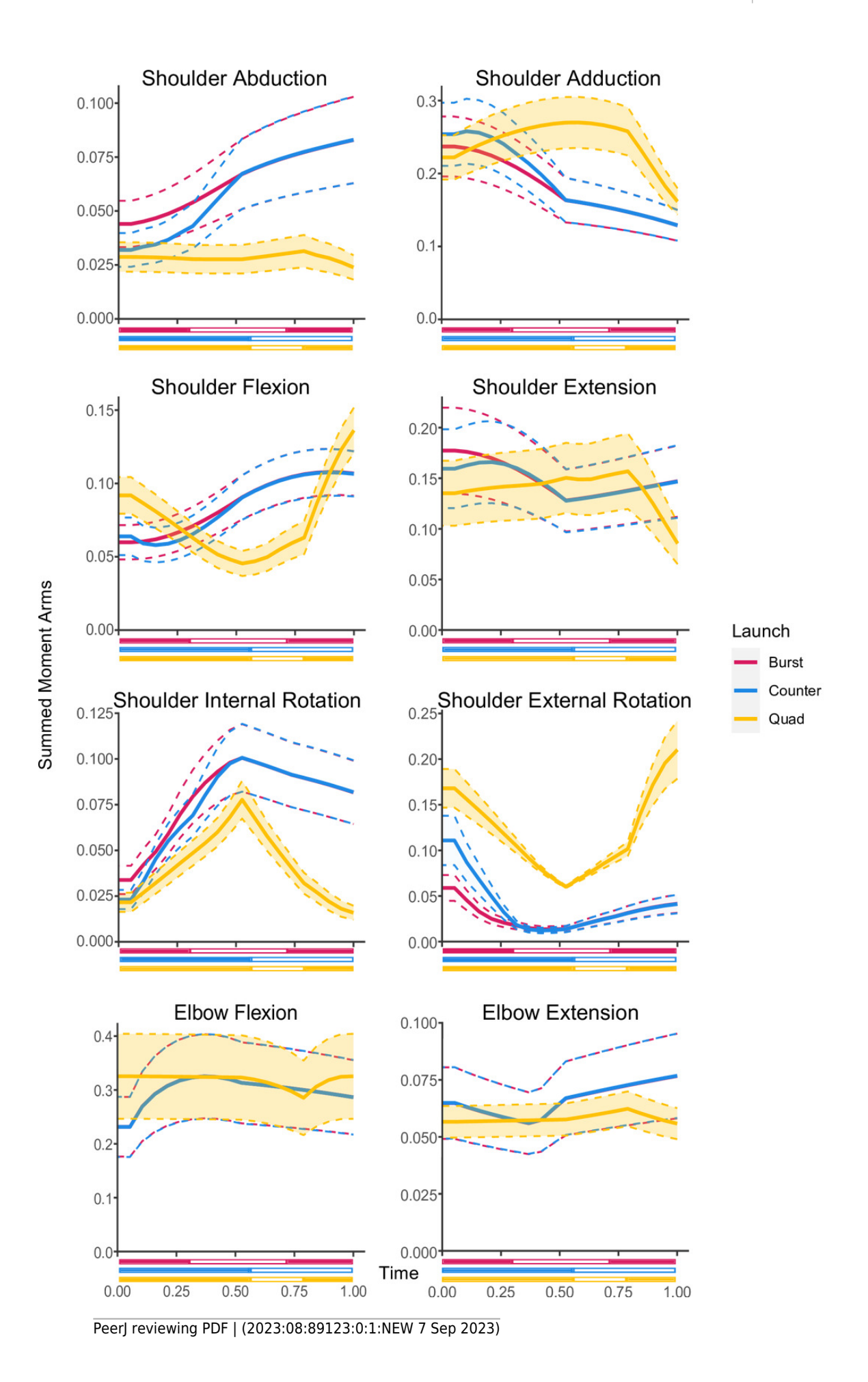




Summed moment arms in each hypothesised take-off motion for the shoulder and elbow rotational DOFs.

Solid lines indicate mean values following Monte Carlo simulation, dashed lines show estimated error, colouration indicates moment arm usage throughout the take-off. Take-off phase markers are equivalent to Figure 2.



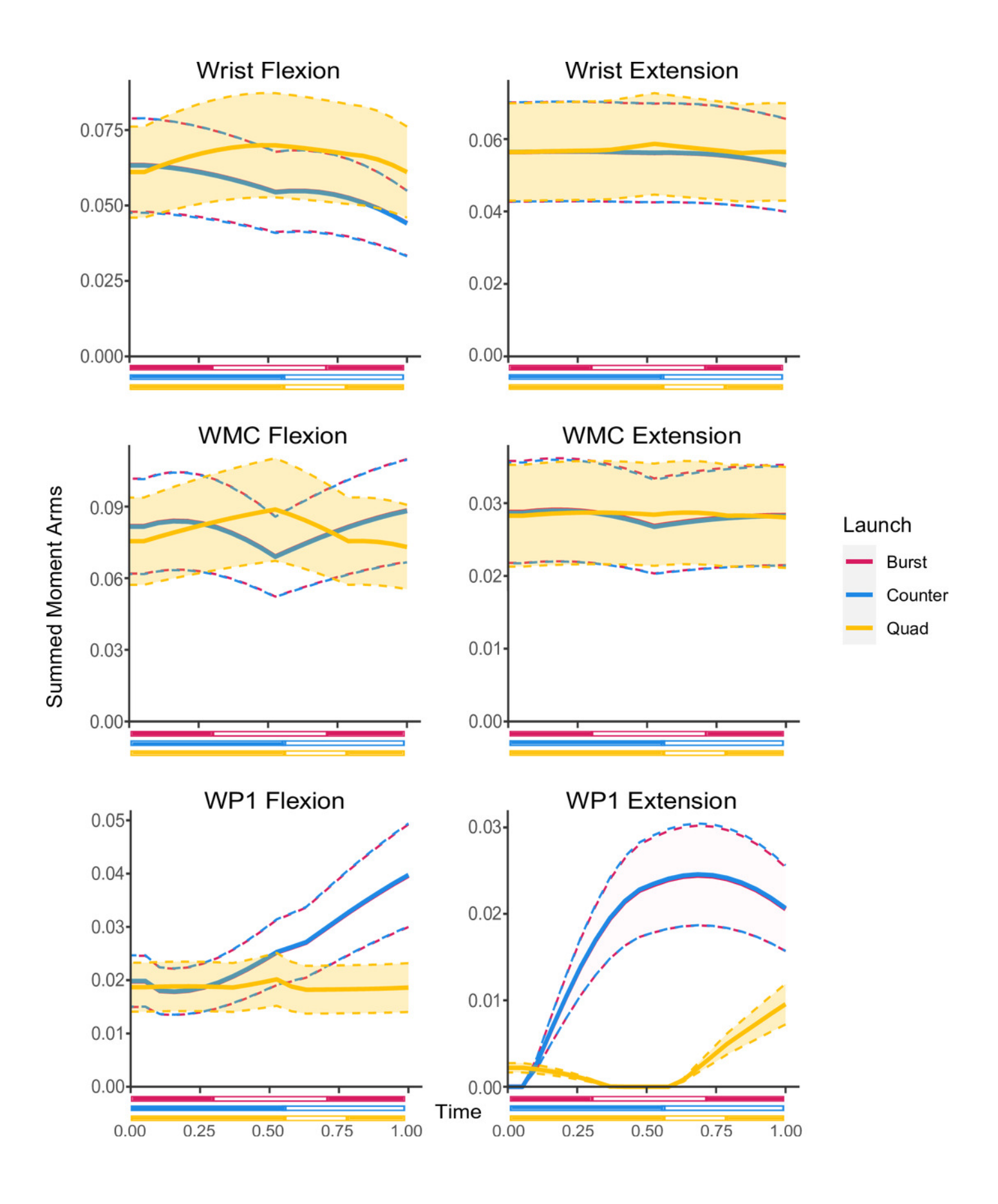




Summed moment arms in each hypothesised take-off motion for the lower forelimb rotational DOFs.

Solid lines indicate mean values following Monte Carlo simulation, dashed lines show estimated error, colouration indicates moment arm usage throughout the take-off. Take-off phase markers are equivalent to Figure 2.







Summed moment arms in each hypothesised take-off motion for the hindlimb rotational DOFs.

Solid lines indicate mean values following Monte Carlo simulation, dashed lines show estimated error, colouration indicates moment arm usage throughout the take-off. Take-off phase markers are equivalent to Figure 2.



